

# Propargylimine in the laboratory and in space: millimetre-wave spectroscopy and its first detection in the ISM<sup>★</sup>

L. Bizzocchi<sup>1</sup>, D. Prudeniano<sup>1</sup>, V. M. Rivilla<sup>2</sup>, A. Pietropolli-Charmet<sup>3</sup>, B. M. Giuliano<sup>1</sup>, P. Caselli<sup>1</sup>,  
J. Martín-Pintado<sup>4</sup>, I. Jiménez-Serra<sup>4</sup>, S. Martín<sup>5,6</sup>, M. A. Requena-Torres<sup>7,8</sup>, F. Rico-Villas<sup>4</sup>,  
S. Zeng<sup>9</sup>, and J.-C. Guillemin<sup>10</sup>

<sup>1</sup> Center for Astrochemical Studies, Max-Planck-Institut für extraterrestrische Physik, Gießenbachstraße 1, 85748 Garching, Germany  
e-mail: [bizzocchi@mpe.mpg.de](mailto:bizzocchi@mpe.mpg.de)

<sup>2</sup> INAF–Osservatorio Astrofisico di Arcetri, Largo Enrico Fermi 5, 50125 Firenze, Italy

<sup>3</sup> Dipartimento di Scienze Molecolari e Nanosistemi, Università Ca' Foscari Venezia, Via Torino 155, 30172 Mestre, Italy

<sup>4</sup> Centro de Astrobiología (CSIC–INTA), Ctra. de Torrejón a Ajalvir, km 4, Torrejón de Ardoz, 28850 Madrid, Spain

<sup>5</sup> European Southern Observatory (ESO), Alonso de Córdoba 3107, Vitacura, 763-0355 Santiago, Chile

<sup>6</sup> Joint ALMA Observatory (ESO), Alonso de Córdoba 3107, Vitacura, 763-0355 Santiago, Chile

<sup>7</sup> University of Maryland, College Park, ND 20742-2421, USA

<sup>8</sup> Department of Physics, Astronomy and Geosciences, Towson University, Towson, MD 21252, USA

<sup>9</sup> Star and Planet Formation Laboratory, Cluster for Pioneering Research, RIKEN, 2-1 Hirosawa, Wako, Saitama 351-0198, Japan

<sup>10</sup> Univ. Rennes, Ecole Nationale Supérieure de Chimie de Rennes, CNRS, ISCR – UMR6226, 35000 Rennes, France

Received 3 April 2020 / Accepted 12 June 2020

## ABSTRACT

**Context.** Small imines containing up to three carbon atoms are present in the interstellar medium (ISM). As alkynyl compounds are abundant in this medium, propargylimine (2-propyn-1-imine,  $\text{HC}\equiv\text{C}-\text{CH}=\text{NH}$ ) thus represents a promising candidate for a new interstellar detection.

**Aims.** The goal of the present work is to perform a comprehensive laboratory investigation of the rotational spectrum of propargylimine in its ground vibrational state in order to obtain a highly precise set of rest frequencies and to search for it in space.

**Methods.** The rotational spectra of *E* and *Z* geometrical isomers of propargylimine have been recorded in the laboratory in the 83–500 GHz frequency interval. The measurements have been performed using a source-modulation millimetre-wave spectrometer equipped with a pyrolysis system for the production of unstable species. High-level ab initio calculations were performed to assist the analysis and to obtain reliable estimates for an extended set of spectroscopic quantities. We searched for propargylimine at 3 mm and 2 mm in the spectral survey of the quiescent giant molecular cloud G+0.693-0.027 located in the central molecular zone, close to the Galactic centre.

**Results.** About 1000 rotational transitions have been recorded for the *E*- and *Z*-propargylimine, in the laboratory. These new data have enabled the determination of a very accurate set of spectroscopic parameters including rotational, quartic, and sextic centrifugal distortion constants. The improved spectral data allowed us to perform a successful search for this new imine in the G+0.693-0.027 molecular cloud. Eighteen lines of *Z*-propargylimine were detected at level  $>2.5\sigma$ , resulting in a column-density estimate of  $N = (0.24 \pm 0.02) \times 10^{14} \text{ cm}^{-2}$ . An upper limit was retrieved for the higher energy *E* isomer, which was not detected in the data. The fractional abundance (with respect to  $\text{H}_2$ ) derived for *Z*-propargylimine is  $1.8 \times 10^{-10}$ . We discuss the possible formation routes by comparing the derived abundance with those measured in the source for possible chemical precursors.

**Key words.** molecular data – methods: laboratory: molecular – methods: observational – techniques: spectroscopic – ISM: clouds – ISM: molecules

## 1. Introduction

Among over 200 molecules detected in the interstellar medium (ISM) and circumstellar shells, approximately 70 have six or more atoms and contain carbon. In an astronomical context, these compounds are called complex organic molecules (COMs, [Herbst & van Dishoeck 2009](#)), and have received increasing attention in the last decade in an effort to unveil how chemical complexity builds up, from simple species to the much larger molecular structures required to establish biochemical

processes on planets where appropriate conditions are met. Nitrogen-bearing COMs are particularly interesting as they can be regarded as an intermediate step towards the formation of biologically significant species, such as nucleobases and amino acids. As protein constituents, amino acids are prime targets for astrobiological studies, and their extraterrestrial formation has been a highly debated topic. Numerous compounds of this class have been found in carbonaceous chondrites (see e.g. [Cobb & Pudritz 2014](#), and references therein), where they are thought to form by aqueous alteration (see [Burton et al. 2012](#) for a review on meteoritic pre-biotic compounds). Glycine, the simplest amino acid, has not been detected in the ISM to date ([Snyder et al. 2005](#)), however it was found in the coma of the 67P/Churyumov–Gerasimenko comet through in situ mass spectrometry

<sup>★</sup> Table of the measured laboratory frequencies is only available at the CDS via anonymous ftp to [cdsarc.u-strasbg.fr](http://cdsarc.u-strasbg.fr) (130.79.128.5) or via <http://cdsarc.u-strasbg.fr/viz-bin/cat/J/A+A/640/A98>

(Altwegg et al. 2016). The presence of glycine in the volatile cometary material thus strongly suggests the existence of a process capable of generating amino acids in cold environments and likely in the absence of liquid water.

Many theoretical and laboratory studies have been devoted to the investigation of the chemical routes that may lead to amino acids in diverse extraterrestrial environments (see e.g. Woon 2002; Koch et al. 2008; Aponte et al. 2017, and references therein). The most promising pathways in interstellar ice analogues involve, as the last step, the hydration of an amino-nitrile compound ( $\text{H}_2\text{N}-\text{CHR}-\text{CN}$ ). In astrophysical-like conditions, these precursors may be generated photochemically, through the addition of ammonia to the corresponding nitrile (Danger et al. 2011a), or via the Strecker mechanism, which starts from the condensation of ammonia with an aldehyde ( $\text{R}-\text{CHO}$ , see Danger et al. 2011b, and references therein). This latter process involves a species containing the iminic moiety ( $\text{RC}=\text{NH}$ ) as reactive intermediate (Aponte et al. 2017).

Imines are a class of molecules that are well represented in the ISM with six members detected to date. Four are simple chains: methanimine ( $\text{CH}_2\text{NH}$ , Godfrey et al. 1973; Dickens et al. 1997), ethanimine ( $\text{CH}_3\text{CHNH}$ , Loomis et al. 2013), ketenimine ( $\text{CH}_2\text{CNH}$ , Lovas et al. 2006), and 3-imino-1,2-propadienylidene ( $\text{CCCNH}$ , Kawaguchi et al. 1992); but there are also the substituted *C*-cyanomethanimine ( $\text{NCCHNH}$ , Zaleski et al. 2013; Rivilla et al. 2019), and the cumulated “diimine” carbodiimide ( $\text{HNCNH}$ , McGuire et al. 2012). Hypotheses on their formation in astrophysical environments point mainly to a chemical route from simple nitriles via tautomerisation (Lovas et al. 2006) or by partial hydrogenation on dust grain surfaces (Theule et al. 2011; Krim et al. 2019).

According to this scheme, it turns out that among the 3C-atom bearing imines, a new, promising candidate for the detection in the ISM would be propargylimine (2-propyn-1-imine,  $\text{HC}\equiv\text{C}-\text{CH}=\text{NH}$ , hereafter PGIM). This species is a structural isomer of the well-known astrophysical molecule acrylonitrile (Gardner & Winnewisser 1970) and can be chemically related — through 2H addition — to cyanoacetylene ( $\text{HC}_3\text{N}$ ), a nitrile species that is ubiquitous in the ISM (e.g. Bizzocchi et al. 2017a, and references therein). Despite this, PGIM has not attracted a great deal of interest from laboratory spectroscopists, and only a few (rather outdated) works are present in the literature. Its rotational spectrum was first observed in 1984 by Kroto et al. (1984) in the centimetre-wave (cm-wave) spectral region. Shortly after, the study was extended by Sugie et al. (1985) and by McNaughton et al. (1988), who also recorded a few rotational transitions for several isotopic variants. In the mid 1980s, the observation of its low-resolution infrared (IR) spectrum was also reported (Hamada et al. 1984; Osman et al. 1987). These few laboratory studies do not provide an exhaustive spectroscopic knowledge. In particular, the coverage of the rotational spectrum is sparse and limited to the cm-wave regime, thus the reliability of the rest frequency computed at millimetre (mm) wavelengths is not suitable for the purpose of an effective astronomical search. With this in mind, we undertook a new extensive laboratory investigation, recording the mm spectrum of PGIM in its vibrational ground state. The newly obtained laboratory data were then used as a point of guidance to search for PGIM towards the quiescent molecular clouds G+0.693-0.027, located in the central molecular zone (CMZ) in the inner ~500 pc of our Galaxy, where several species directly related to pre-biotic chemistry have recently been detected (Requena-Torres et al. 2006, 2008; Zeng et al. 2018; Jiménez-Serra et al. 2020).

The structure of the paper is as follows. In Sect. 2, we describe the experimental procedure, and in Sect. 3, we provide a short account of the theoretical calculations performed to support the data analysis. In Sect. 4, we describe the spectral analysis and discuss the results. In Sect. 5, we describe the observations performed to search for PGIM in the ISM and illustrate the analysis of the data which leads to its positive identification. Finally, we draw our conclusions in Sect. 6.

## 2. Experiments

The rotational spectrum of PGIM has been recorded using the CASAC (Center for Astrochemical Studies Absorption Cell) spectrometer at the Max-Planck-Institut für extraterrestrische Physik in Garching. Full details on the experimental setup have already been provided (Bizzocchi et al. 2017b); here, we report only a few key details that apply to the present investigation. The instrument employs an active multiplier chain (Virginia Diodes) as a source of mm radiation in the 82–125 GHz band. This primary stage is driven by a cm-wave synthesiser that operates in the 18–28 GHz frequency range. Accurate frequency and phase stabilisation is achieved by locking the parent cm synthesiser to an Rb atomic clock. With the use of further multiplier stages in cascade, the frequency coverage can be extended towards the sub-mm regime with the available power of a 2–20  $\mu\text{W}$  up to 1 THz. A closed-cycle He-cooled InSb hot electron bolometer operating at 4 K (QMC) is used as a detector. The spectral measurements were performed using the frequency modulation (FM) technique: the carrier signal from the cm-wave synthesiser is sine-wave modulated at 50 kHz, and the detector output is demodulated at twice this frequency ( $2f$ ) by a lock-in amplifier. The second derivative of the actual absorption profile is thus recorded by the computer-controlled acquisition system.

The absorption cell is a plain Pyrex tube (3 m long and 5 cm in diameter), which at one end is connected to a side arm hosting a pyrolysis production system. This consists of a quartz tube (1 cm in diameter, 60 cm long) inserted in a tubular oven (Carbolite) that heats up the inner 40 cm long part.

Propargylimine was produced as in Sugie et al. (1985). We pyrolysed dipropargylamine ( $(\text{HC}\equiv\text{CCH}_2)_2\text{NH}$ ) vapours and flowed the gaseous reaction products through the absorption cell, which was continuously pumped. In our setup, the strongest absorption signals of the target molecule were obtained by setting the oven temperature at 950°C. The typical pressure was 150–200 mTorr (20–26 Pa) at the quartz tube inlet. This corresponds to about 4 mTorr (0.5 Pa) in the absorption cell, which was kept at room temperature. Multiple by-products were formed, as reported by McNaughton et al. (1988), occasionally generating strong spectral features. This, however, did not hamper the recording of the PGIM spectrum, thus sample purification via selective trapping or condensation/re-vaporisation were not attempted in the present investigation.

## 3. Molecular properties

PGIM can be described as a molecule joining two basic sub-units: the ethynyl group  $\text{HC}\equiv\text{C}-$  and the iminic moiety  $-\text{CH}=\text{NH}$ . The presence of two conjugated multiple bonds forces the molecule to the planar configuration with all the seven atoms lying on the plane defined by the *a* and *b* principal axes. Owing to different relative positions of the HCC group and of the iminic H with respect to the C=N double bond, two structural isomers exist: *Z* and *E*. Their structures are depicted in Fig. 1.

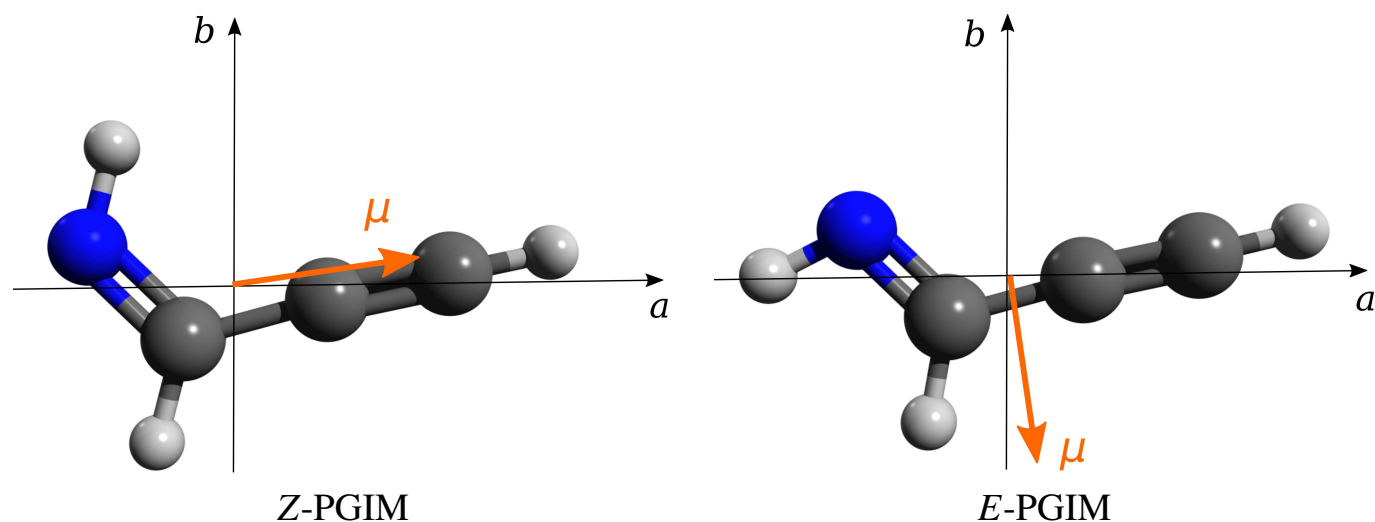


**Fig. 1.** Molecular structure and principal inertial axes of the *Z* and *E* isomers of PGIM. The orange arrow indicates the direction of the electric dipole moment  $\mu$  and points towards the displacement of the notional negative charge. The modulus is  $\mu = 2.15$  D for *Z*-PGIM and  $\mu = 1.95$  D for *E*-PGIM.

With the aim of fully characterising the molecular properties of the PGIM, we conducted extensive theoretical calculations at the coupled-cluster (CC) level of the theory, with single and double excitation augmented by a perturbative treatment for estimating the effects of triple excitation (i.e. CCSD(T), Raghavachari et al. 1989). Appropriate extrapolation procedures to the complete basis set (CBS) limit (Heckert et al. 2005a,b) were then employed to estimate the equilibrium structures of the two conformers and their energies. Employing a similar composite approach (see e.g. Barone et al. 2015; Pietropoli Charmet et al. 2017a; Degli Esposti et al. 2018) the best-estimate values of the quadratic force fields were derived. Cubic and semi-diagonal quartic force constants, computed at different levels of theory, were employed for the vibrational corrections to the equilibrium rotational constants, for the anharmonic corrections to the harmonic frequencies, and for determining the sextic centrifugal distortion constants. Nuclear quadrupole coupling constants for the nitrogen atoms were computed following the same procedure described previously (Cazzoli et al. 2011; Pietropoli Charmet et al. 2016). Additional details on the calculations (levels of theory, basis sets, and methodology) are reported in the Appendix A.

From our calculations, the energy difference between the *Z* (more stable) and *E* isomers is  $0.8510 \text{ kcal mol}^{-1}$  ( $E/k = 428.2 \text{ K}$ ). Both isomers are prolate-type slightly asymmetric tops ( $\kappa \sim 0.98$ ). While the modulus of the dipole moment is similar ( $|\mu| \sim 2 \text{ D}$ ), the corresponding components in the principal axes are very different:  $\mu_a = 2.14 \text{ D}$  and  $\mu_b = 0.17 \text{ D}$  for the *Z* isomer;  $\mu_a = 0.26 \text{ D}$  and  $\mu_b = 1.93 \text{ D}$  for the *E* isomer. The dipole moment vectors are also shown in Fig. 1.

#### 4. Spectral analysis

The rotational spectrum of PGIM was recorded in selected frequency intervals from 83 to 500 GHz. In the mm region, *Z*-PGIM presents a typical *a*-type spectrum with groups of *R*-branch  $\Delta K_a = 0$  transitions regularly separated by  $\approx B + C$ , (Fig. 2, upper panel), while the *E* isomer exhibits a much more complex spectrum consisting of several overlapping  $\Delta K_a \pm 1$  ladders with some prominent *Q*-branch band heads spaced by  $\approx 2A - B - C$  (Fig. 2, lower panel).

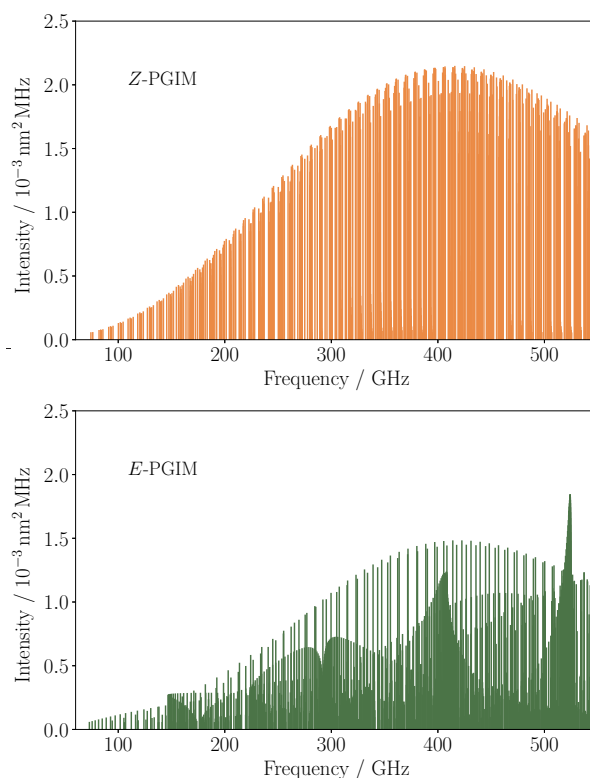


**Fig. 2.** Stick spectra of *Z* (upper panel) and *E* (lower panel) isomers of PGIM computed at 300 K. Frequency positions and intensities were computed using the spectroscopic parameters reported in Table 2 and the ab initio values of the dipole moments (see Appendix A).

From the ab initio computed energy difference, a relative  $[Z]/[E]$  isomer abundance of 4.2 can be estimated at 300 K. From the relative intensity comparison between a pair of nearby *Z*- and *E*-PGIM lines recorded under the same experimental conditions (source power, sample pressure, and modulation depth) we obtained  $[Z]/[E] = 4.7 \pm 0.7$ , in good agreement with the theoretical computation. This indicates that, although PGIM is generated in a high-temperature environment ( $\sim 950 \text{ }^\circ\text{C}$ ), there is

**Table 1.** Summary of the transitions with resolved hyperfine structure recorded for both PGIM isomers.

Z-PGIM				E-PGIM			
Type <sup>(a)</sup>	No. of lines	No. of comp. <sup>(b)</sup>	$K'_a$	Type <sup>(a)</sup>	No. of lines	No. of comp. <sup>(b)</sup>	$K'_a$
<sup>a</sup> $R_{0,+1}$	29	76	0,1,2,3	<sup>b</sup> $P_{+1,-1}$	10	18	1
<sup>b</sup> $R_{+1,+1}$	4	6	0	<sup>b</sup> $R_{0,+1}$	73	140	0,1,2
<sup>b</sup> $R_{-1,+1}$	3	6	1	<sup>b</sup> $Q_{+1,-1}$	50	99	0,1,2
<sup>b</sup> $Q_{+1,-1}$	6	12	0				

**Notes.** <sup>(a)</sup>See footnote on page 4. <sup>(b)</sup>Resolved hyperfine components.

a quick thermalisation between the two isomers, and the population relaxes to the 300 K value right after the gas comes into contact with the cell walls.

Due to the presence of nitrogen, hyperfine coupling is generated between the molecular electric field gradient averaged over the end-over-end rotation, and the quadrupole moment of the  $^{14}\text{N}$  nucleus with a spin of  $I = 1$ . Thus, each rotational level with a principal quantum number of  $J > 0$  is split into three hyperfine sub-levels labelled with the total angular quantum number  $F$ , where  $F = J - 1, J, J + 1$ . As a consequence, the transitions are split into several components according to the  $\Delta F = 0, \pm 1$  selection rules, with the strongest features being those for which  $\Delta F = \Delta J$ . However, in the frequency interval covered by the present investigation, the  $J$  quantum number reaches a value as high as 54, thus most of the <sup>a</sup> $R_{0,+1}$  transitions<sup>1</sup> (which dominate the Z isomer spectrum) have their hyperfine pattern collapsed into a single feature. Nevertheless, for a few low- $J$  lines it was possible to detect the very weak  $\Delta F = 0$  components, which form a widely separated doublet approximately centred at the frequency of the corresponding unsplit transition. An example of such hyperfine patterns is given in Fig. 3. The situation is different for the  $b$ -type lines, which is typical of the E isomer spectrum. Due to the change in the  $K_a$  pseudo quantum number involved in these transitions, less tight hyperfine patterns are produced, and doublets or triplets of lines have generally been recorded, as shown in Fig. 4. A summary of the transitions of both isomers for which the hyperfine structures have been resolved is presented in Table 1.

Whenever possible, each measured feature was assigned to a single quadrupole component. Close patterns were observed as a single line, and in this case the intensity-averaged calculated frequency (typically of two or three components) was compared with the experimental datum in the least-squares fit. Loose blends of unresolved components were also observed. These lines appeared as broad and distorted features and were not used in the analysis. This careful selection procedure made it possible to achieve the same measurement precision for both the singly-assigned and for the intensity-averaged hyperfine entries. A sizeable number of recorded transitions did not show any hint of hyperfine splitting, namely 381 for the Z isomer and 288 for the E isomer. For these data, the contributions resulting from the nuclear quadrupole coupling were neglected, and the measured frequencies were assigned to the corresponding pure rotational transitions. For each isomer, lines with or without resolved

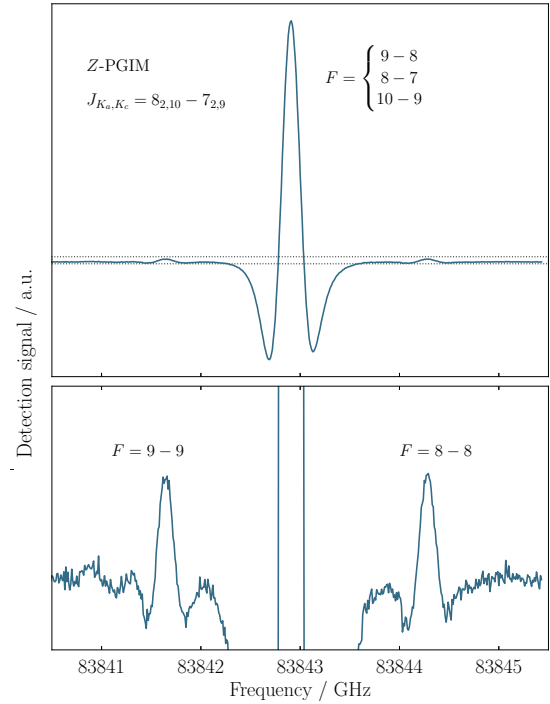


**Fig. 3.** Recording of the  $J_{K_a, K_c} = 8_{2,10} - 7_{2,9}$  of Z-PGIM showing the two weak  $\Delta F = 0$  hyperfine components symmetrically separated from the central blended  $\Delta F = +1$  triplet by 1.3 MHz (upper panel). Total integration time of 47 s with time constant  $RC = 3$  ms. The area enclosed in the dashed box is plotted with an expanded  $y$ -axis in the lower panel.

hyperfine structure were given the same assumed uncertainty and analysed together in a global least-squares fashion.

In total, our data sets comprise 531 lines for Z-PGIM and 545 lines for E-PGIM. They also included 50 and 47 cm-wave transitions, respectively, taken from the literature (Sugie et al. 1985; McNaughton et al. 1988). Different statistical weights  $w = 1/\sigma^2$  were given to the data of the various sub-sets to take into account the different measurement precision ( $\sigma$ ). For the lines measured by Sugie et al. (1985), we retained the same weighting scheme of the original paper, while 50 kHz was given to the few transitions of the Z isomer reported by McNaughton et al. (1988). The average uncertainty of the frequencies measured in the present work is estimated to be 15 kHz. The complete data list is provided in electronic form at the CDS.

The hyperfine energies were computed adopting the standard vector coupling scheme between the rotational angular momentum  $\mathbf{J}$  and the nitrogen spin  $\mathbf{I}_N$ :

$$\mathbf{J} + \mathbf{I}_N = \mathbf{F}. \quad (1)$$

<sup>1</sup> The symbol  ${}^x M_{\delta K_a, \delta K_c}$  is used to succinctly label the transition type of an asymmetric rotor:  $x$  indicates the dipole moment component involved,  $M = P, Q, R$  is the symbol for the transitions with  $\Delta J = -1, 0, +1$ , respectively, and  $\delta K_a$  and  $\delta K_c$  refer to the (signed) change of the  $K_a$  and  $K_c$  pseudo-angular quantum numbers (Gordy & Cook 1984).

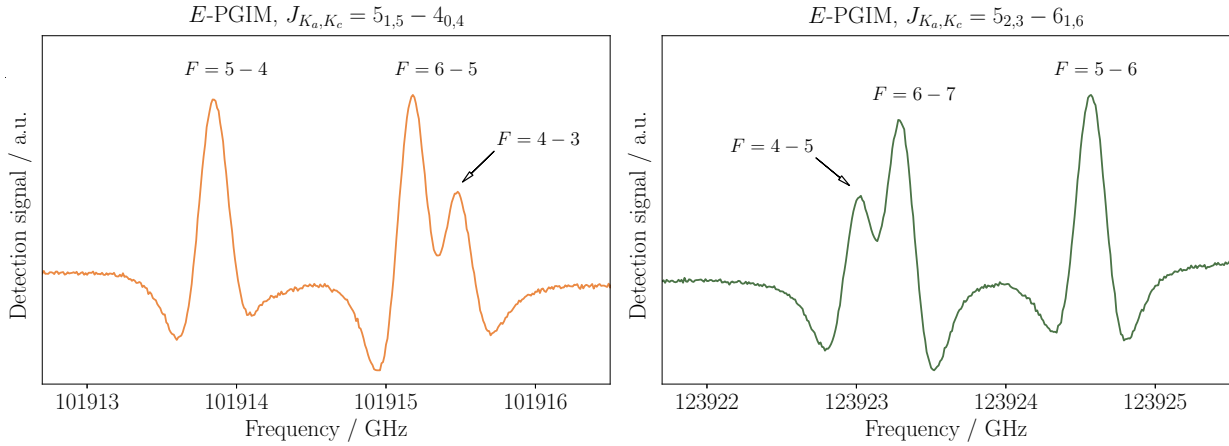


**Fig. 4.** Recordings of two  $b$ -type transitions for  $E$ -PGIM showing the typical hyperfine structure produced by the quadrupole coupling of the  $^{14}\text{N}$  nucleus. *Left panel:*  $J_{K_a, K_c} = 5_{1,5} - 4_{0,4}$ ; integration time 180 s. *Right panel:*  $J_{K_a, K_c} = 5_{2,3} - 6_{1,6}$ ; integration time 165 s. The adopted scan rate is  $0.2 \text{ MHz s}^{-1}$  with time constant  $RC = 3 \text{ ms}$ .

The total Hamiltonian is thus expressed as the sum of a purely rotational part and a hyperfine contribution:

$$\hat{H} = \hat{H}_{\text{rot}} + \hat{H}_{\text{HFS}}. \quad (2)$$

The pure rotational levels are labelled with the quantum numbers  $J_{K_a, K_c}$ , and the total angular momentum quantum number,  $F$ , must be added when the hyperfine sub-levels are considered. The rotational Hamiltonian  $\hat{H}_{\text{rot}}$  is the  $S$ -reduced Watson-type Hamiltonian in its  $I'$  representation (Watson 1977a) and includes centrifugal distortion corrections up to the octic terms. The hyperfine-structure Hamiltonian,  $\hat{H}_{\text{HFS}}$ , is expressed by the traceless tensor  $\chi$ , which has  $\chi_{aa}$  and  $\chi_{bb} - \chi_{cc}$  as determinable coefficients. This term has been considered only for the analysis of the resolved hyperfine components. The weak spin-rotation couplings of both  $^{14}\text{N}$  and H nuclei do not produce any detectable effect in the recorded spectra and were thus neglected. All spectral computations were performed with the CALPGM suite of programs (Pickett 1991).

The spectroscopic parameters for the two propargylimine isomers are reported in Table 2, together with a compilation of theoretically computed quantities derived as described in Appendix A. Very precise determinations of the rotational constants  $A, B, C$  were obtained, of which the uncertainties are reduced by factors of 7–30 compared to the ones obtained in the previous study (Sugie et al. 1985). The quartic centrifugal distortion constants had also been determined in that work, but using an approximated perturbation expression (described in Watson 1967), so they are not directly comparable with the present results. The precision of our determined values is very high: the standard errors are generally of a few  $10^{-3}\%$ , only  $D_K$  for the Z isomer – for which mainly  $a$ -type transition were recorded – reaches 0.07%. A full set of sextic centrifugal distortion constants have been obtained for the first time, and their uncertainties are generally less than 1% (12% for  $H_K$  of the Z isomer). Additionally, two octic centrifugal distortion constants ( $L_{JJK}$ ,  $L_{JK}$  for the Z isomer and  $L_{JK}$ ,  $L_{JKK}$  for the E isomer) had to be included in the fit in order to reproduce all the measured transition frequencies within the experimental accuracy. Their values should be considered as “effective”, and they are determined with at least 15% uncertainty.

The comparison between experimentally derived and theoretically computed values shows an overall excellent agreement. For the rotational constants, the deviations are generally lower

than 0.1%; the quartic centrifugal distortion coefficients show an average absolute deviation of less than 5% for both isomers, with only the small  $d_2$  constants showing larger deviations. Also, the sextic centrifugal distortion constants compare well with the corresponding ab initio predictions; in all but a few cases, the deviations are within 10%. Notable exceptions are the  $H_K$  and  $h_3$  values for the Z isomer, for which only a few  $b$ -type transitions were recorded, thus making these parameters highly correlated with the much larger  $A$  and  $D_K$  constants.

The theoretically computed values of the quadrupole coupling tensor components are also very close to the ones derived from the experimental hyperfine structure analysis. In general, they agree within 3–4%; only  $\chi_{aa}$  for the E isomer is slightly off ( $\sim 10\%$ ), but its experimental value is also affected by a larger uncertainty and it is consistent with the ab initio prediction within  $3\sigma$ .

From the spectroscopic parameters presented in Table 2, we generated reliable sets of rest frequencies to guide astronomical PGIM searches in the ISM. To evaluate the overall precision of our spectral computations, we chose a sub-set of transitions with  $K_a = 0, 1, 2, 3$  and lower level energy,  $E/k < 200 \text{ K}$ . Then, we further singled out all the lines with integrated intensities of at least  $1/10$  of the maximum computed at 50 K. These selections constitute the most critical spectral data for an effective search for the PGIM isomers in astrophysical sources. They contain 159 lines in the 54–265 GHz range for Z-PGIM, and 247 lines in the 66–551 GHz range for the E-PGIM. The maximum  $1\sigma$  errors are 1.9 and 4.7 kHz, respectively, which corresponds to radial equivalent velocity uncertainties in the ranges  $0.8 - 2.0 \times 10^{-2} \text{ km s}^{-1}$  at 3 mm, and  $0.3 - 0.8 \times 10^{-2} \text{ km s}^{-1}$  at 1 mm regime.

As electronic supplementary information (available at the CDS), we provide a set of spectral catalogues for PGIM isomers directly obtained with the SPCAT program (Pickett 1991) without any further editing. They match the CDMS<sup>2</sup> (Müller et al. 2005; Endres et al. 2016) and JPL<sup>3</sup> (Pickett et al. 1998) file format exactly, and are thus suited for direct use in widespread astronomy line-analysis tools, such as CASSIS<sup>4</sup> and MAD-CUBA (Rivilla et al. 2016). For each isomer, the results of two separate computations are provided. The x-pgim.cat files

<sup>2</sup> <https://cdms.astro.uni-koeln.de/cdms>

<sup>3</sup> <http://spec.jpl.nasa.gov/>

<sup>4</sup> CASSIS is a software package for the analysis of astronomical spectra developed by IRAP-UPS/CNRS (<http://cassis.irap.omp.eu>).

**Table 2.** Experimental and theoretical spectroscopic parameters of PGIM isomers.

Parameter	Z-PGIM		E-PGIM		
	Exp.	Ab initio <sup>(a)</sup>	Exp.	Ab initio <sup>(a)</sup>	
<i>A</i>	/MHz	54 640.1468(45)	54 713.513	63 099.2207(22)	63 096.337
<i>B</i>	/MHz	4862.362758(60)	4858.512	4766.557614(55)	4764.532
<i>C</i>	/MHz	4458.249970(55)	4455.474	4425.560983(58)	4423.690
<i>D<sub>J</sub></i>	/kHz	2.008283(40)	2.021	1.608429(49)	1.604
<i>D<sub>JK</sub></i>	/kHz	−101.1809(21)	−103.4	−108.8303(15)	−113.9
<i>D<sub>K</sub></i>	/MHz	4.1783(39)	4.132	6.19213(63)	6.452
<i>d<sub>1</sub></i>	/kHz	−0.410926(21)	−0.412	−0.3010587(82)	−0.301
<i>d<sub>2</sub></i>	/kHz	−0.027954(24)	−0.0239	−0.0188128(25)	−0.0154
<i>H<sub>J</sub></i>	/mHz	5.5695(83)	5.688	4.035(13)	3.925
<i>H<sub>JK</sub></i>	/Hz	−0.4629(80)	−0.4464	−0.46703(77)	−0.4788
<i>H<sub>KJ</sub></i>	/Hz	−6.733(28)	−7.879	−3.690(47)	−3.192
<i>H<sub>K</sub></i>	/kHz	3.28(39)	0.7938	1.042(46)	1.101
<i>h<sub>1</sub></i>	/mHz	2.1716(70)	2.189	1.5502(23)	1.486
<i>h<sub>2</sub></i>	/mHz	0.3385(63)	0.2721	0.2059(11)	0.165
<i>h<sub>3</sub></i>	/mHz	0.1202(45)	0.0733	0.06093(23)	0.0450
<i>L<sub>JJK</sub></i>	/μHz	3.06(38)	–	–	–
<i>L<sub>JK</sub></i>	/mHz	−0.3330(28)	–	−0.3403(98)	–
<i>L<sub>KKJ</sub></i>	/mHz	–	–	−2.11(32)	–
<i>χ<sub>aa</sub></i>	/MHz	−4.0641(61)	−4.1900	1.035(39)	0.9311
<i>χ<sub>bb</sub> − χ<sub>cc</sub></i>	/MHz	−2.654(15)	−2.7758	−7.6632(96)	−7.8950
<i>σ<sub>w</sub></i>		0.91		0.88	
No. of lines		531		545	

**Notes.** Numbers in parentheses are  $1\sigma$  statistical uncertainties in the units of the last quoted digit. <sup>(a)</sup>Equilibrium constants from extrapolated best structure, zero-point vibrational corrections computed at fc-MP2/aug-cc-pVTZ. Quartic centrifugal distortion constants computed using a composite scheme. Sextic centrifugal distortion constants computed at fc-CCSD(T)/cc-pVTZ. Nuclear quadrupole coupling constants computed at the ae-CCSD(T)/cc-pwCV5Z level. See Appendix A for further explanation.

contain a listing of pure rotational frequencies extending up to 600 GHz, whereas the `x-pgim_hfs.cat` files provide a list of hyperfine components limited to 200 GHz. The first character (`x`) of the file names takes the values `z` or `e` according to which isomer the file refers to. In all catalogues, the integrated intensity of each transition is computed at 300 K in order to comply with the CDMS standard.

A selection of rotational ( $Q_{\text{rot}}$ ), hyperfine ( $Q_{\text{HFS}}$ ), and vibrational ( $Q_{\text{vib}}$ ) partition functions for PGIM isomers is provided in Table 3. The values are computed for temperatures in the 3–300 K interval, and they are obtained by direct summation over the rotational or hyperfine levels of which the energy position is accurately determined during the spectral analysis. The vibrational partition functions are computed through direct summation on all energy levels (including combinations and overtones), which give a fractional contribution to  $Q_{\text{vib}}$  higher than  $10^{-7}$ .

## 5. Detection of PGIM in the Galactic centre cloud G+0.693

### 5.1. Observations

We searched for PGIM towards the molecular cloud G+0.693-0.027 (G+0.693 hereafter) located in the CMZ, the inner ~500 pc

of our Galaxy. G+0.693, located at ~1 arcmin north-east of the star-forming protocluster SgrB2(N), does not show any sign of ongoing massive star formation such as H<sub>2</sub>O masers, H II regions, or dust continuum sources (e.g. Ginsburg et al. 2018). However, despite being a quiescent cloud, it is one of the main repositories of COMs in the Galaxy (Requena-Torres et al. 2008; Zeng et al. 2018). Among the many molecules detected in this cloud, there are several species directly related to pre-biotic chemistry like the simplest sugar glycolaldehyde (CH<sub>2</sub>OHCHO; Requena-Torres et al. 2006), formamide and methyl isocyanate (NH<sub>2</sub>CHO and CH<sub>3</sub>NCO, respectively; Zeng et al. 2018), phosphorous-bearing species such as PO (Rivilla et al. 2018), and recently urea (NH<sub>2</sub>CONH<sub>2</sub>, Jiménez-Serra et al. 2020). In addition, several imines have been reported towards G+0.693: methanimine (CH<sub>2</sub>NH, Zeng et al. 2018), ethanimine (CH<sub>3</sub>CHNH, Rivilla, in prep.), and the *E,Z* isomers of *C*-cyanomethanimine, NCCHNH, NCCHNH (Rivilla et al. 2019), a possible precursor of adenine, which is one of the DNA and RNA nucleobases. For Z-NCCHNH, this is the first detection in the ISM. Therefore, G+0.693 is a promising target for the detection of new imines such as PGIM.

We searched for PGIM in a spectral survey of G+0.693 conducted with the IRAM 30 m telescope at 3 and 2 mm. The observations were performed during two different observing runs in 2019: April 10-16 (project 172-18), and August 13-19

**Table 3.** Rotational, hyperfine, and vibrational partition functions for PGIM isomers.

$T/K$	Z-PGIM			E-PGIM		
	$Q_{\text{rot}}$	$Q_{\text{HFS}}$	$Q_{\text{vib}}$	$Q_{\text{rot}}$	$Q_{\text{HFS}}$	$Q_{\text{vib}}$
3	26.073	78.218	1.0000	24.593	73.779	1.0000
5	55.562	166.69	1.0000	52.409	157.23	1.0000
10	156.05	468.14	1.0000	147.20	441.59	1.0000
15	286.02	858.06	1.0000	269.81	809.43	1.0000
25	614.37	1843.11	1.0000	579.58	1738.72	1.0000
50	1736.09	5208.26	1.0026	1637.91	4913.72	1.0022
100	4911.56	14 734.7	1.0674	4634.74	13 904.21	1.0637
150	9028.77	27 086.3	1.2375	8520.22	25 560.7	1.2301
225	16 602.6	49 807.8	1.7010	15 634.8	46 904.5	1.6883
300	25 569.7	76 708.8	2.5137	23 925.1	71 774.9	2.4962

(project 018-19). We used the broad-band Eight MIXer Receiver (EMIR) and the fast Fourier transform spectrometers in FTS200 mode, which provided a channel width of  $\sim 200$  kHz, meaning a velocity resolution of  $\sim 0.35$ – $0.85$  km s $^{-1}$ . Since we are interested in weak line emissions, we smoothed all the spectra to  $5$  km s $^{-1}$  velocity resolution, enough to resolve the line widths of  $\sim 20$  km s $^{-1}$  measured in this source. Each spectral setup was observed several times slightly changing the central frequency (by 20–100 MHz shifts) in order to identify possible spectral features resulting from unsuppressed image side-band emission.

## 5.2. Data analysis and results

The two intervals of frequency covered by the survey are 71.76–116.72 GHz and 124.77–175.5 GHz. During the observations, the pointing was checked every 1–1.5 h on nearby planets, QSOs or bright H II regions, and the telescope focus was checked at the beginning of the observations and after sunset and sunrise. The half-power beam width (HPBW) of the telescope at the observed frequencies is  $14''$ – $33''$ . The observations were centred at the coordinates of G+0.693:  $\alpha$ (J2000) =  $17^{\text{h}}47^{\text{m}}22^{\text{s}}$  and  $\delta$ (J2000) =  $-28^{\circ}21'27''$ . The position switching mode was used in all the observations, with an off position of ( $-885''$ ,  $290''$ ). The line intensity of the spectra is given in  $T_{\text{A}}^*$  as the molecular emission towards G+0.693 is extended over the full beam (Requena-Torres et al. 2006; Martín et al. 2008; Rivilla et al. 2018). Contamination by image-band lines was identified and eliminated during data reduction, comparing the same frequency band observed with two different spectral setups.

The identification of the molecular lines was performed using the new spectroscopic PGIM data and the Spectral Line Identification and Modelling (SLIM) tool within the MAD-CUBA package<sup>5</sup> (Martín et al. 2019). The SLIM tool generates synthetic spectra of molecular species under the assumption of local thermodynamic equilibrium (LTE) conditions. We used the MADCUBA-AUTOFIT tool that compares the observed spectra with LTE synthetic spectra, and provides the best non-linear least-squares fit using the Levenberg-Marquardt algorithm (see details in Martín et al. 2019). The free parameters of the fit are:

<sup>5</sup> Madrid Data Cube Analysis on ImageJ software was developed at the Centre of Astrobiology (CAB) in Madrid; <http://cab.inta-csic.es/madcuba/Portada.html>

the molecular column density ( $N$ ), the excitation temperature ( $T_{\text{ex}}$ ), the systemic velocity ( $v_{\text{LSR}}$ ), and the full width at half maximum (FWHM) of the line Gaussian profiles. Since the fit convergence was difficult to achieve when trying to optimise all four parameters, we fixed the  $v_{\text{LSR}}$  and the FWHM to 69 and 20 km s $^{-1}$ , respectively. These values allowed us to reproduce all the observed spectra well, and they are consistent with the ones derived for other imines in the same source (Zeng et al. 2018; Rivilla et al. 2019). We also fixed the excitation temperature to 8 K, as found for C-cyanomethanimine (Rivilla et al. 2019), as well as for other complex organic molecules (Requena-Torres et al. 2006, 2008). This value also compares well to that obtained for the simplest imine, CH $_2$ NH, which was  $9.7 \pm 0.4$  K (Zeng et al. 2018).

The 18 brightest transitions of Z-PGIM detected in our data at level  $>2.5\sigma$  are illustrated in Fig. 5. The resulting line parameters are summarised in Table 4. For each transition, we evaluated the possible blending with other molecular species. We searched the spectral survey for more than 300 different molecules, which include all the species detected so far in the ISM<sup>6</sup>. The complete list of the molecular species detected in the survey will be presented in a forthcoming paper. Within the scope of this work, in Fig. 5 we show the contribution of the molecules identified in the spectral intervals around the transitions assigned for Z-PGIM. We note that the low excitation temperature of the COMs detected in this source guarantees that only the lowest energy levels of these molecules are populated (see Table 4). This implies that line confusion is expected to be less severe in this source than in hot core sources such as SgrB2(N) (e.g. Belloche et al. 2019) in spite of the larger line widths. Therefore, the level of line blending of the molecular lines, especially at 3 mm, is expected to be low.

We ran AUTOFIT to derive the column density of Z-PGIM using the transitions that are less blended with other species (indicated with an asterisk in Table 4). The resulting simulated spectra are presented in red solid lines in Fig. 5. The Z-PGIM transitions have integrated intensities  $\int T_{\text{A}}^* dv > 68$  mK km s $^{-1}$  (see Table 4). We calculated the detection level of each transition by comparing the velocity-integrated intensity with  $\sigma = \text{rms} \times \sqrt{\delta v / \text{FWHM}} \times \text{FWHM}$ . Here, the noise root mean square (rms) is measured over a line-free spectral range of  $\pm 500$  km s $^{-1}$

<sup>6</sup> <https://cdms.astro.uni-koeln.de/classic/molecules>.

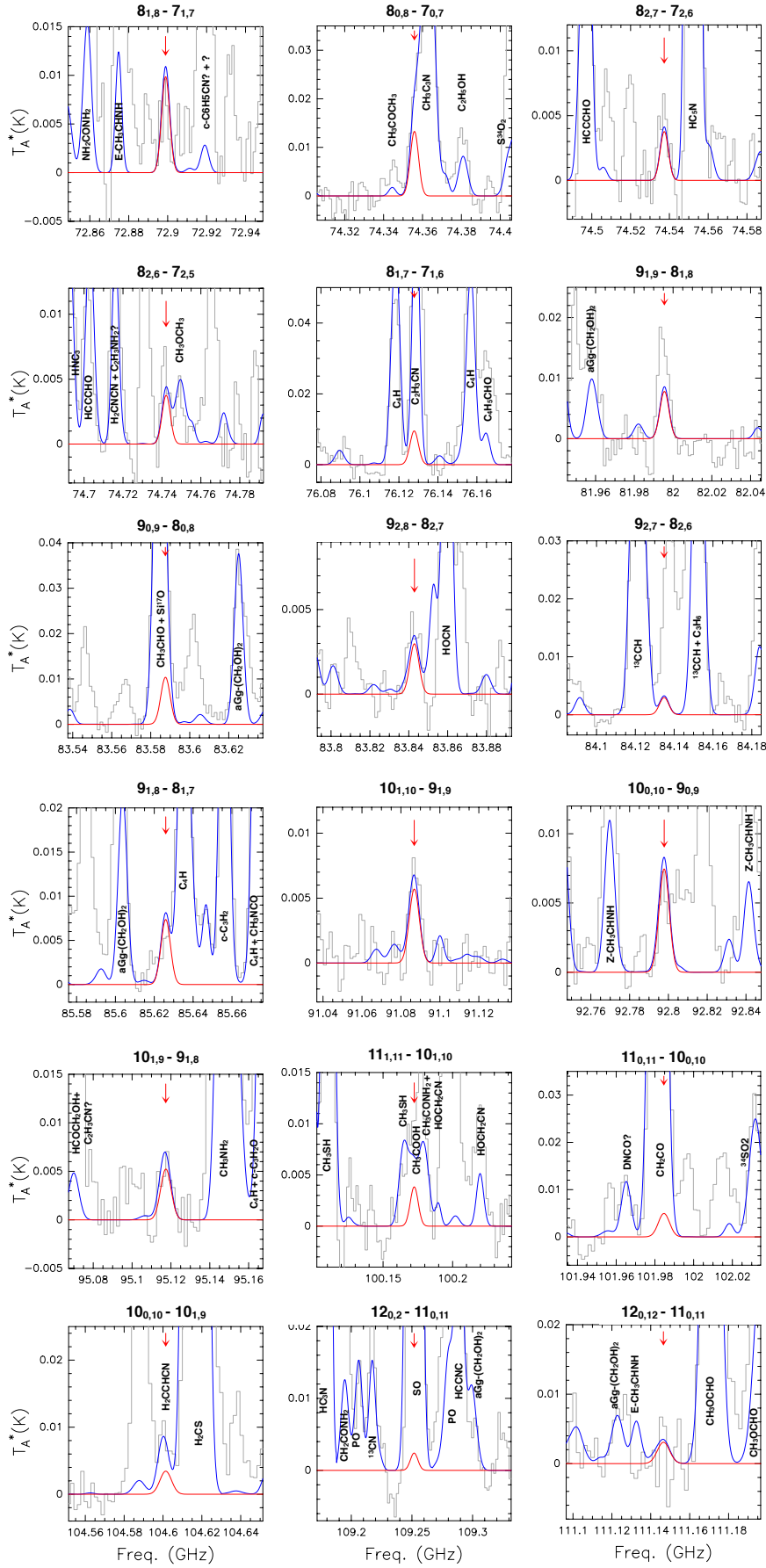


**Fig. 5.** LTE spectrum (in red) of the 18 brightest transitions of Z-PGIM detected towards G+0.693. The contributions of all the species identified in the source so far are indicated with a blue curve.

**Table 4.** Transitions of Z-PGIM detected towards G+0.693.

Frequency <sup>(a)</sup> (GHz)	Transition	$\log I$ <sup>(b)</sup> (nm <sup>2</sup> MHz)	$E_{\text{up}}$ (cm <sup>-1</sup> )	$\int T_{\text{A}}^* dv$ (mK km s <sup>-1</sup> )	Detection level <sup>(c)</sup>
72.898955*	8 <sub>1,8</sub> –7 <sub>1,7</sub>	–4.315	10.18	281	8.0
74.355828*	8 <sub>0,8</sub> –7 <sub>0,7</sub>	–4.288	8.70	378	16.4
74.537358*	8 <sub>2,7</sub> –7 <sub>2,6</sub>	–4.328	15.37	107	4.2
74.742197*	8 <sub>2,6</sub> –7 <sub>2,5</sub>	–4.325	15.38	107	4.6
76.127838	8 <sub>1,7</sub> –7 <sub>1,6</sub>	–4.278	10.56	271	9.9
81.995559*	9 <sub>1,9</sub> –8 <sub>1,8</sub>	–4.166	12.61	222	8.0
83.587572	9 <sub>0,9</sub> –8 <sub>0,8</sub>	–4.141	11.18	295	13.5
83.842907*	9 <sub>2,8</sub> –8 <sub>2,7</sub>	–4.174	17.86	84	4.3
84.134809	9 <sub>2,7</sub> –8 <sub>2,6</sub>	–4.171	17.87	84	4.1
85.625901*	9 <sub>1,8</sub> –8 <sub>1,7</sub>	–4.129	13.10	209	5.4
91.086864*	10 <sub>1,10</sub> –9 <sub>1,9</sub>	–4.034	15.35	162	10.1
92.797807*	10 <sub>0,10</sub> –9 <sub>0,9</sub>	–4.010	13.96	212	14.1
95.117382*	10 <sub>1,9</sub> –9 <sub>1,8</sub>	–3.997	15.95	149	7.0
100.172426*	11 <sub>1,11</sub> –10 <sub>1,10</sub>	–3.916	18.39	109	3.0
101.984662	11 <sub>0,11</sub> –10 <sub>0,10</sub>	–3.894	17.06	141	4.7
104.601405*	11 <sub>1,10</sub> –10 <sub>1,9</sub>	–3.880	19.13	98	3.0
109.251842	12 <sub>1,12</sub> –11 <sub>1,11</sub>	–3.809	21.73	68	3.2
111.146539	12 <sub>0,12</sub> –11 <sub>0,11</sub>	–3.789	20.46	87	2.7

**Notes.** <sup>(a)</sup>Asterisks denote the transitions used in the MADCUBA–AUTOFIT analysis. <sup>(b)</sup>Base 10 logarithm of the integrated intensity of the transition at 300 K. <sup>(c)</sup>See Sect. 5.2.

**Table 5.** Derived physical parameters for PGIM isomers and proposed molecular precursors.

Molecule	$N$ (10 <sup>14</sup> cm <sup>-2</sup> )	$T_{\text{ex}}$ (K)	$v_{\text{LSR}}$ (km s <sup>-1</sup> )	$FWHM$ (km s <sup>-1</sup> )	Abundance <sup>(a)</sup> (×10 <sup>-10</sup> )	Reference
Z-PGIM	0.24 ± 0.02	8	69	20	1.8	1
<i>E</i> -PGIM	<0.13	8	69	20	<0.9	1
CH <sub>3</sub> CCH <sup>(b)</sup>	17.0 ± 2	19 ± 1	69	20	126	1
HC <sub>3</sub> N <sup>(c)</sup>	7.1 ± 1.3	12 ± 2	68 ± 1	22 ± 1	53	2
CH <sub>2</sub> CHCN	0.9 ± 0.1	10.8 ± 1.1	68 ± 1	22 ± 2	7	2
CCH <sup>(c)</sup>	53 ± 7	–	–	–	391	1
Z-NCCHNH	2.0 ± 0.6	8 ± 2	68.3 ± 0.8	20	15	3
<i>E</i> -NCCHNH	0.33 ± 0.03	8	68.0 ± 0.8	21 ± 2	2.4	3
HCCCHO	0.32 ± 0.02	18 ± 2	67.6 ± 0.4	20	2.4	4

**Notes.** <sup>(a)</sup>We adopted  $N_{\text{H}_2} = 1.35 \times 10^{23}$  cm<sup>-2</sup> as inferred by Martín et al. (2008) from C<sup>18</sup>O observations. <sup>(b)</sup>Fit obtained from the  $J = 9 - 8, 8 - 7, 6 - 5$  and  $5 - 4$  transitions with  $K = 0$  and  $K = 1$ . <sup>(c)</sup>The column densities of HC<sub>3</sub>N and CCH were derived from the optically thin transitions of the H<sup>13</sup>CCCN and C<sup>13</sup>CH isotopologues, respectively. The isotopic ratio of <sup>12</sup>C/<sup>13</sup>C ~ 21 measured by Armijos-Abendaño et al. (2015) in G+0.693 was used.

**References.** (1) This work; (2) Zeng et al. (2018); (3) Rivilla et al. (2019); (4) Rivilla (in prep.).

around each transition, and  $\delta v$  is the spectral resolution expressed in velocity units. The derived rms are in the 1.5–3.9 mK km s<sup>-1</sup> range in channels of 5 km s<sup>-1</sup>. As indicated in Table 4, 14 transitions are detected above  $4\sigma$ , and eight transitions are above  $6\sigma$ . The integrated intensities corresponding to the fitted column densities derived by AUTOFIT are shown in Table 5. The column density of Z-PGIM is  $(0.24 \pm 0.02) \times 10^{14}$  cm<sup>-2</sup>. By considering the H<sub>2</sub> column density towards G+0.693,

$N_{\text{H}_2} = 1.35 \times 10^{23}$  cm<sup>-2</sup> (Martín et al. 2008), we can derive a Z-PGIM fractional abundance of  $1.8 \times 10^{-10}$ .

The higher-energy *E*-PGIM isomer is not detected in the data. To derive its upper limit, we used the two brightest spectral features that appear completely free of contamination by other species in the observed spectra: the hyperfine  $\Delta F = +1$  triplet of the  $J_{K_a, K_c} = 5_{1,5} - 4_{0,4}$  line centred at 101 915 MHz ( $E_L = 3.07$  cm<sup>-1</sup>), and the one of the  $J_{K_a, K_c} = 6_{1,6} - 5_{0,5}$  line at

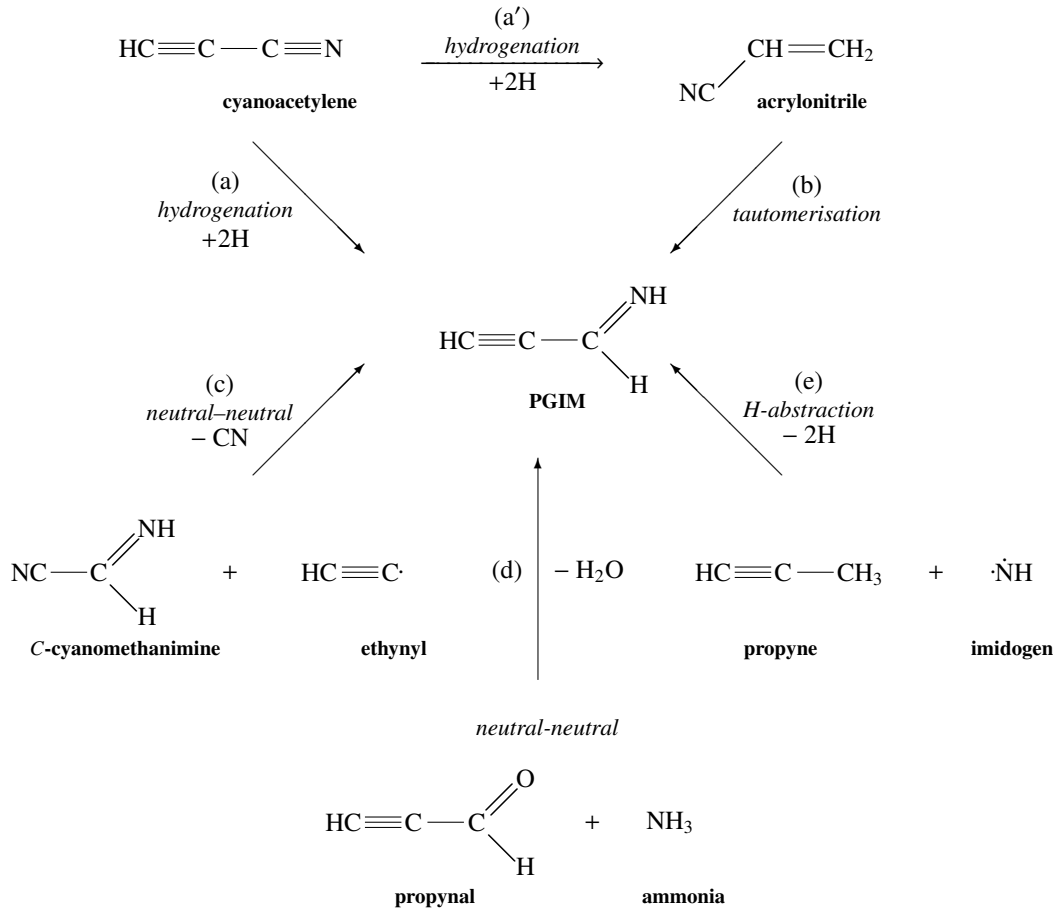


**Fig. 6.** Possible formation mechanisms of PGIM in the ISM.

110 103 GHz ( $E_L = 4.60 \text{ cm}^{-1}$ ). We adopted the same assumptions on excitation temperature, velocity, and line FWHM as for the Z-PGIM. The upper limits to the integrated intensity are derived using the formula  $3 \times \text{rms} \times \Delta v / \sqrt{n_{\text{chan}}}$ , where  $n_{\text{chan}}$  is the number of channels covered by the full line width  $\Delta v$ . The upper limit derived for the column density of E-PGIM is  $N < 1.3 \times 10^{13} \text{ cm}^{-2}$ . This implies an isomer abundance ratio of  $[Z]/[E] > 1.9$ , hinting at a higher abundance of the thermodynamically more stable form.

We also report fractional abundances of other molecular species that might be chemically related to PGIM: cyanoacetylene ( $\text{HC}_3\text{N}$ ), acrylonitrile ( $\text{CH}_2\text{CHCN}$ ), propyne ( $\text{CH}_3\text{CCH}$ ), C-cyanomethanimine ( $\text{NCCHNH}$ ), ethynyl ( $\text{CCH}$ ), and propynal ( $\text{HCCCHO}$ ). All of them are detected towards G+0.693 and have abundances  $\geq 10^{-9}$ . The derived parameters are presented in Table 5. For  $\text{CH}_3\text{CCH}$ , we fitted the  $J = 9-8, 8-7, 6-5$  and  $5-4$  transitions with  $K = 0, 1$ . For  $\text{CCH}$ , we derived its abundance by fitting the optically thin lines of the isotopic variant  $\text{C}^{13}\text{CH}$ , and assuming the isotopic ratio of  $^{12}\text{C}/^{13}\text{C} \sim 21$  measured in G+0.693 by Armijos-Abendaño et al. (2015). For  $\text{HC}_3\text{N}$ ,  $\text{CH}_3\text{CHCN}$ , and  $\text{NCCHNH}$ , we adopted the values obtained in previous works (Zeng et al. 2018; Rivilla et al. 2019), whereas the  $\text{HCCCHO}$  results are taken from a full chemical analysis of the source that will be presented in a forthcoming paper (Rivilla, in prep.).

### 5.3. Discussion

To the best of our knowledge, the formation of PGIM in the ISM has not been investigated to date, thus there are no chemical

pathways included in astrochemical databases such as KIDA<sup>7</sup> (Wakelam et al. 2012) or UMIST<sup>8</sup> (McElroy et al. 2013). In the following, we formulate and discuss a few possible PGIM formation mechanisms based on the results of theoretical and experimental studies of detected imines (e.g. Lovas et al. 2006; Theule et al. 2011; Krim et al. 2019):

- (a) hydrogenation of cyanoacetylene (possibly on dust grains);
- (b) tautomerisation of acrylonitrile;
- (c) neutral–neutral reaction between C-cyanomethanimine and the ethynyl radical to form PGIM and the CN radical;
- (d) reaction of propynal and ammonia followed by water elimination;
- (e) hydrogen abstraction on propyne, which gives PGIM after reaction with the imidogen radical.

The schematic reactions are illustrated in Fig. 6. As shown in Table 5, all the proposed processes involve molecular precursors that are significantly more abundant than PGIM (although propynal only marginally), therefore it is not unlikely that one (or several) of these mechanisms might be able to account for the presence of this imine in G+0.693.

Route (a) involves selective hydrogenation of the  $\text{C}\equiv\text{N}$  group on dust grain surfaces. This process has proven to be effective for generating fully saturated methylamine from HCN ices (Theule et al. 2011), although the intermediate imine was not observed. More doubtful is the viability of this chemical scheme starting from larger nitriles. For example, the formation of ethanimine

<sup>7</sup> <http://kida.obs.u-bordeaux1.fr>

<sup>8</sup> <http://udfa.ajmarkwick.net/index.php>

from CH<sub>3</sub>CN, as suggested by Loomis et al. (2013), seems to be unlikely in view of recent laboratory works (Nguyen et al. 2019), which investigated the co-deposition of methyl cyanide and H atoms and showed that the C≡N moiety is not reduced in the 10–60 K temperature range. In the absence of energetic processes, the hydrogenation of cyanocetylene would result in a competition of the H attack to the C≡C and C≡N triple bonds, leading mainly to acrylonitrile (Krim et al. 2019, route a'). However, route (a) cannot be completely ruled out, as the chemistry in G+0.693 is known to be shock dominated (e.g. Rivilla et al. 2019). Also, the cosmic-ray ionisation rate is expected to be high across the Galactic centre (Goto et al. 2013), as well as in G+0.693 (see Zeng et al. 2018), thus providing an additional source of energy.

Route (b) is analogous to the proposed CH<sub>3</sub>CN→CH<sub>2</sub>=C=NH conversion driven by shocks (Lovas et al. 2006). The energetics of the Z-PGIM→CH<sub>2</sub>=CHCN tautomerisation was investigated theoretically by Osman et al. (2014). Their calculations (at the MP2 level of theory) show that acrylonitrile is more stable than Z-PGIM by 32.7 kcal mol<sup>-1</sup> ( $E/k \approx 16\,500$  K), and the double H migration involved in the process has barrier energies exceeding 80 kcal mol<sup>-1</sup> ( $E/k \approx 40\,300$  K). They concluded that CH<sub>2</sub>=CHCN is dominant in the cold ISM, and point to a conversion to PGIM possibly occurring in shock-dominated regions or hot cores. The above figures however, seem to be too high to allow for such a pathway in the shocks affecting G+0.693 (Requena-Torres et al. 2006).

Routes (c), (d), and (e), require two molecules to be co-spatial. In all these processes, at least one reactant is much more abundant than PGIM in G+0.693: (ethynyl, propyne, and ammonia), hence they are feasible in principle. Route (d) seems to be less likely, because propynal is only marginally more abundant than PGIM, unlike the other two reactants, C-cyanomethanimine and propyne, which are factors of ~10 and ~100 more abundant, respectively. However, given the lack of information on the associated reaction rates and energy barriers, only speculative reasoning can be done.

In analogous cases, hints to constrain the formation scenario can be provided by the observed [Z]/[E] isomer abundance ratio. It has been proposed that the relative abundances of structural isomers in the ISM might be established by their thermodynamic stability (minimum energy principle, see Lattelais et al. 2009). Although there are some well-known exceptions (H<sub>4</sub>C<sub>2</sub>O<sub>2</sub> and H<sub>2</sub>C<sub>3</sub>O isomers; see also Shingledecker et al. 2019), this hypothesis seems to work well, at least for simple cases of geometrical isomerism. Rivilla et al. (2019), for example, showed that the ratio between the Z- and E- isomers of C-cyanomethanimine (NCCHNH) does follow thermodynamic equilibrium:

$$[Z]/[E] = \frac{N(Z)}{N(E)} = \frac{1}{g} \exp\left(\frac{\Delta E}{T_k}\right), \quad (3)$$

where  $\Delta E$  is the energy difference between the two isomers,  $T_k$  is the kinetic temperature of the gas, and  $g$  is a factor that accounts for statistical weights (1 for the Z- and E- isomers of both NCCHNH and PGIM). The [Z]/[E] ~ 6 found for C-cyanomethanimine implies a  $T_k$  in the 130–210 K range, which is in good agreement with the kinetic temperature measured by Zeng et al. (2018) in G+0.693<sup>9</sup>.

<sup>9</sup> The  $T_k$  value found for G+0693 is significantly lower than the average  $T_{\text{ex}}$  of the observed molecules (see Table 5), as, due to the low density of the source, their rotational energy level manifolds are sub-thermally populated.

According to our newly performed ab initio calculations (see Appendix A), the  $\Delta E/k$  for PGIM isomers is 428.2 K. Using this value, the [Z]/[E] ratio expected for PGIM for the  $T_k$  range 130–210 K, is 8–27. This prediction is consistent with the observed lower limit of [Z]/[E] > 1.9, but the lack of a more stringent upper limit for E-PGIM prevents a firm confirmation that PGIM isomers actually follow the relative abundance predicted by thermodynamics.

The cosmic-ray ionisation rate in the CMZ where G+0.693 is located is expected to be a factor of 10–100 higher in the Galactic centre than in the disc, as measured by Goto et al. (2013, 2014) using H<sub>3</sub><sup>+</sup> observations. Zeng et al. (2018) suggested that a relatively high cosmic-ray ionisation rate of  $1\text{--}10 \times 10^{-15} \text{ s}^{-1}$  might be responsible of the cyanopolyyne and nitrile molecular ratios found in G+0.693. Indeed, this produces an enhanced abundance of C atoms, due to the efficient CO destruction (Bisbas et al. 2019), possibly accounting for the large abundance of carbon chains in this region. Also, a high cosmic-ray ionisation rate can efficiently create atomic hydrogen (H) via the dissociation of H<sub>2</sub> (Padovani et al. 2018); then, different reactivity levels of the PGIM isomers with atomic H might produce the different abundances observed. However, theoretical quantum chemical calculations of the reactions of PGIM isomers with H need to be performed to test this possibility.

Another possible destruction route is through charged species such as H<sub>3</sub><sup>+</sup>. In this case, the destruction rates depend on the permanent dipole moment of the different isomers. For C-cyanomethanimine, the E isomer presents a dipole moment that is a factor of ~3 higher than the one of the Z isomer. Shingledecker et al. (2020) has shown theoretically that this produces a more efficient destruction of the E through a reaction with H<sub>3</sub><sup>+</sup>, which may contribute to its lower abundance observed in G+0.693. This explanation, however, cannot be applied to PGIM, since both Z and E isomers have very similar moduli of their permanent dipole moments (see Sect. 3). Therefore, one should expect similar destruction rates for both isomers with H<sub>3</sub><sup>+</sup>.

## 6. Conclusions

This paper presents an extensive theoretical and laboratory study of the rotational spectrum of PGIM in its vibrational ground state, extending the earlier, very limited knowledge on the spectroscopic properties of this simple imine. The recordings were performed in selected frequency intervals spanning the 83–500 GHz range, collecting some 500 lines for each of the two E and Z geometrical isomers. These experimental data were fitted to the coefficients of the S-reduced rotational Hamiltonian, providing a very precise set of rotational, quartic, and sextic centrifugal distortion constants. Many transitions, especially b-type dipole ones, show resolvable hyperfine patterns due to the quadrupole coupling of the <sup>14</sup>N nuclei. For these transitions, 357 separate components were accurately measured and analysed to determine the corresponding hyperfine coupling coefficients. The optimised values of all the spectroscopic constants are in excellent agreement with the results of high-level theoretical calculations, which were performed to assist the analysis of the laboratory data.

The newly obtained set of spectroscopic parameters (Table 2) allowed us to generate a highly precise set of rest frequencies for E- and Z-PGIM at the mm regime. With these data, we searched for PGIM in a spectral survey of the molecular cloud G+0.693 located in the CMZ. We detected 18 transitions of Z-PGIM, the lowest energy isomer, for which a column density of  $N = (0.24 \pm 0.02) \times 10^{14} \text{ cm}^{-2}$  was derived. The higher energy

E-PGIM isomer was not detected in the data, setting an upper limit of  $N < 1.3 \times 10^{13} \text{ cm}^{-2}$  from the two strong spectral features, which show no contamination from other species.

The fractional abundance (with respect to  $\text{H}_2$ ) derived for Z-PGIM is  $1.8 \times 10^{-10}$ . This value was compared with the ones found for possible chemical precursors including cyanoacetylene ( $\text{HC}_3\text{N}$ ), propyne ( $\text{CH}_3\text{CCH}$ ), acrylonitrile ( $\text{CH}_2\text{CHCN}$ ), C-cyanomethanimine ( $\text{NCCHNH}$ ), ethynyl ( $\text{CCH}$ ), and propynal ( $\text{HCCCHO}$ ). The relative abundances of all of them detected towards G+0.693 are higher (by up to two orders of magnitude for  $\text{CH}_3\text{CCH}$ ) than that of PGIM.

**Acknowledgements.** We thank the IRAM-30m staff for the precious help during the different observing runs. A.P.C. gratefully acknowledges financial support by University Cà Foscari Venezia (ADiR funds) and the super-computing facilities of CINECA (project “CINEMA”, grant HP10C2QE6F) and SCSCF (“Sistema per il Calcolo Scientifico di Cà Foscari”, a multiprocessor cluster system owned by Università Cà Foscari Venezia). V.M.R. has received funding from the European Union’s Horizon 2020 research and innovation programme under the Marie Skłodowska-Curie grant agreement No 664931. I.J.-S. and J.M.-P. have received partial support from the Spanish FEDER (project number ESP2017-86582-C4-1-R), and State Research Agency (AEI) through project number MDM-2017-0737 Unidad de Excelencia María de Maeztu—Centro de Astrobiología (INTA-CSIC). J.C.G. thanks the program Physique et Chimie du Milieu Interstellaire (INSU-CNRS), the Centre National d’Etudes Spatiales (CNES) and the PHC Procope 42516WC (CAMPUS France) for financial support. D.P. and L.B. acknowledge DAAD support through the project 57445281 “Small organic molecules in the Interstellar Medium” in the framework of “Programm Projektbezogener Personenaustausch Frankreich (Phase I) 2019”. S.Z. acknowledges support from RIKEN Special Postdoctoral Researcher Program.

## References

- Aliiev, M. R., & Watson, J. K. G. 1976, *J. Mol. Spectrosc.*, **61**, 29
- Aliiev, M. R., & Watson, J. K. G. 1985, in *Molecular Spectroscopy: Modern Research*, ed. K. N. Rao, Vol. III (New York: Academic Press), 1
- Altwegg, K., Balsiger, H., Bar-Nun, A., et al. 2016, *Sci. Adv.*, **2**, e1600285
- Aponte, J. C., Elsila, J. E., Glavin, D. P., et al. 2017, *ACS Earth Space Chem.*, **1**, 3
- Armijos-Abendaño, J., Martín-Pintado, J., Requena-Torres, M. A., Martín, S., & Rodríguez-Franco, A. 2015, *MNRAS*, **446**, 3842
- Bak, K. L., Gauss, J., Jørgensen, P., et al. 2001, *J. Chem. Phys.*, **114**, 6548
- Barone, V., Biczysko, M., & Puzzarini, C. 2015, *Acc. Chem. Res.*, **48**, 1413
- Belloche, A., Garrod, R. T., Müller, H. S. P., et al. 2019, *A&A*, **628**, A10
- Bisbas, T. G., Schrubba, A., & van Dishoeck, E. F. 2019, *MNRAS*, **485**, 3097
- Bizzocchi, L., Tamassia, F., Laas, J., et al. 2017a, *ApJS*, **233**, 11
- Bizzocchi, L., Lattanzi, V., Laas, J., et al. 2017b, *A&A*, **602**, A34
- Burton, A. S., Stern, J. C., Elsila, J. E., Glavin, D. P., & Dworkin, J. P. 2012, *Chem. Soc. Rev.*, **41**, 5459
- Cazzoli, G., Cludi, L., Puzzarini, C., et al. 2011, *J. Phys. Chem. A*, **115**, 453
- Cobb, A. K., & Pudritz, R. E. 2014, *ApJ*, **783**, 140
- Danger, G., Bossa, J. B., de Marcellus, P., et al. 2011a, *A&A*, **525**, A30
- Danger, G., Borget, F., Chomat, M., et al. 2011b, *A&A*, **535**, A47
- Degli Esposti, C., Dore, L., Puzzarini, C., et al. 2018, *A&A*, **615**, A176
- Dickens, J. E., Irvine, W. M., De Vries, C. H., & Ohishi, M. 1997, *ApJ*, **479**, 307
- Dunning, Jr., T. H. 1989, *J. Chem. Phys.*, **90**, 1007
- Endres, C. P., Schlemmer, S., Schilke, P., Stutzki, J., & Müller, H. S. P. 2016, *J. Mol. Spectrosc.*, **327**, 95
- Gambi, A., Pietropoli Charmet, A., Stoppa, P., et al. 2019, *Phys. Chem. Chem. Phys.*, **21**, 3615
- Gardner, F. F., & Winnewisser, G. 1970, *ApJ*, **195**, L127
- Gauß, J., & Stanton, J. F. 1997, *Chem. Phys. Lett.*, **276**, 70
- Ginsburg, A., Bally, J., Barnes, A., et al. 2018, *ApJ*, **853**, 171
- Godfrey, P. D., Brown, R. D., Robinson, B. J., & Sinclair, M. W. 1973, *ApL*, **13**, 119
- Gordy, W., & Cook, R. L. 1984, *Microwave Molecular Spectra* (New York: John Wiley & Sons)
- Goto, M., Indriolo, N., Geballe, T. R., & Usuda, T. 2013, *J. Phys. Chem. A*, **117**, 9919
- Goto, M., Geballe, T. R., Indriolo, N., et al. 2014, *ApJ*, **786**, 96
- Halkier, A., Helgaker, T., Jørgensen, P., Klopper, W., & Olsen, J. 1999, *Chem. Phys. Lett.*, **302**, 437
- Hamada, Y., Tsuboi, M., Takeo, H., & Matsumura, C. 1984, *J. Mol. Spectrosc.*, **106**, 175
- Heckert, M., Kállay, M., & Gauss, J. 2005a, *Mol. Phys.*, **103**, 2109
- Heckert, M., Kállay, M., Tew, D. P., Klopper, W., & Gauss, J. 2005b, *J. Chem. Phys.*, **125**, 044108
- Helgaker, T., Klopper, W., Koch, H., & Noga, J. 1997a, *J. Chem. Phys.*, **106**, 9639
- Helgaker, T., Gauss, J., Jørgensen, P., & Olsen, J. 1997b, *J. Chem. Phys.*, **106**, 9430
- Herbst, E., & van Dishoeck, E. F. 2009, *ARA&A*, **47**, 427
- Jiménez-Serra, I., Martín-Pintado, J., Rivilla, V. M., et al. 2020, *Astrobiology*, in press, <https://doi.org/10.1089/ast.2019.2125>
- Kawaguchi, K., Takano, S., Ohishi, M., et al. 1992, *ApJ*, **396**, L49
- Kendall, R. A., Dunning, T. H., & Harrison, R. J. 1992, *J. Chem. Phys.*, **96**, 6796
- Koch, D. M., Toubin, C., Peslherbe, G. H., & Hynes, J. T. 2008, *J. Phys. Chem. C*, **112**, 2972
- Krim, L., Guillemin, J.-C., & Woon, D. E. 2019, *MNRAS*, **485**, 5210
- Kroto, H. W., McNaughton, D., & Osman, I. O. 1984, *J. Chem. Soc. Chem. Comm.*, 993
- Lattelais, M., Pauzat, F., Ellinger, Y., & Ceccarelli, C. 2009, *ApJ*, **696**, L133
- Loomis, R. A., Zaleski, D. P., Steber, A. L., et al. 2013, *ApJ*, **765**, L9
- Lovas, F. J., Hollis, J. M., Remijan, A. J., & Jewell, P. R. 2006, *ApJ*, **645**, L137
- Martín, S., Requena-Torres, M. A., Martín-Pintado, J., & Mauersberger, R. 2008, *ApJ*, **678**, 245
- Martín, S., Martín-Pintado, J., Blanco-Sánchez, C., et al. 2019, *A&A*, **631**, A159
- McCarthy, M. C., Martinez, O., McGuire, B. A., et al. 2016, *J. Chem. Phys.*, **144**, 124304
- McElroy, D., Walsh, C., Markwick, A. J., et al. 2013, *A&A*, **550**, A36
- McGuire, B. A., Loomis, R. A., Charness, C. M., et al. 2012, *ApJ*, **758**, L33
- McNaughton, D., Osman, O. I., & Kroto, H. W. 1988, *J. Mol. Struct.*, **190**, 195
- Møller, C., & Plesset, M. S. 1934, *Phys. Rev.*, **46**, 618
- Müller, H. S. P., Schlöder, F., Stutzki, J., & Winnewisser, G. 2005, *J. Mol. Struct.*, **742**, 215
- Nguyen, T., Fourré, I., Favre, C., et al. 2019, *A&A*, **628**, A15
- Osman, I. O., McNaughton, D., Suffolk, R. J., Watts, J. D., & Kroto, H. W. 1987, *J. Chem. Soc. Perkin Trans. II*, 683
- Osman, O. I., Elroby, S. A., Aziz, S. G., & Hilal, R. H. 2014, *Int. J. Mol. Sci.*, **15**, 11064
- Padovani, M., Galli, D., Ivlev, A. V., Caselli, P., & Ferrara, A. 2018, *A&A*, **619**, A144
- Peterson, K. A., & Dunning, T. H. 2002, *J. Chem. Phys.*, **117**, 10548
- Pickett, H. M. 1991, *J. Mol. Spectrosc.*, **148**, 371
- Pickett, H. M., Poynter, R. L., Cohen, E. A., et al. 1998, *J. Quant. Spectr. Rad. Transf.*, **60**, 883
- Pietropoli Charmet, A., & Cornaton, Y. 2018, *J. Mol. Struct.*, **1160**, 455
- Pietropoli Charmet, A., Stoppa, P., Tasinato, N., et al. 2010, *J. Chem. Phys.*, **133**, 044310
- Pietropoli Charmet, A., Stoppa, P., Tasinato, N., Giorgianni, S., & Gambi, A. 2016, *J. Phys. Chem. A*, **120**, 8369
- Pietropoli Charmet, A., Stoppa, P., Giorgianni, S., et al. 2017a, *J. Phys. Chem. A*, **121**, 3305
- Pietropoli Charmet, A., Stoppa, P., Tasinato, N., & Giorgianni, S. 2017b, *J. Mol. Spectrosc.*, **335**, 117
- Puzzarini, C., Biczysko, M., Bloino, J., & Barone, V. 2014, *ApJ*, **785**, 107
- Raghavachari, K., Trucks, G. W., Pople, J. A., & Head-Gordon, M. 1989, *Chem. Phys. Lett.*, **157**, 479
- Ramabhadran, R. O., & Raghavachari, K. 2013, *J. Chem. Theor. Comp.*, **9**, 3986
- Requena-Torres, M. A., Martín-Pintado, J., Rodríguez-Franco, A., et al. 2006, *A&A*, **455**, 971
- Requena-Torres, M. A., Martín-Pintado, J., Martín, S., & Morris, M. R. 2008, *ApJ*, **672**, 352
- Rivilla, V. M., Fontani, F., Beltrán, M. T., et al. 2016, *ApJ*, **862**, 161
- Rivilla, V. M., Jiménez-Serra, I., Zeng, S., et al. 2018, *MNRAS*, **475**, L30
- Rivilla, V. M., Martín-Pintado, J., Jiménez-Serra, I., et al. 2019, *MNRAS*, **483**, L114
- Shingledecker, C. N., Álvarez-Barcia, S., Korn, V. H., & Kästner, J. 2019, *ApJ*, **878**, 80
- Shingledecker, C. N., Molpeceres, G., Rivilla, V., Majumdar, L., & Kästner, J. 2020, *ApJ*, **897**, 158
- Snyder, L. E., Lovas, F. J., Hollis, J. M., et al. 2005, *ApJ*, **619**, 914
- Sugie, M., Takeo, H., & Matsumura, C. 1985, *J. Mol. Spectrosc.*, **111**, 83
- Theule, P., Borget, F., Mispelaer, F., et al. 2011, *A&A*, **534**, A64
- Wakelam, V., Herbst, E., Loison, J.-C., et al. 2012, *ApJS*, **199**, 21
- Watson, J. K. G. 1967, *J. Chem. Phys.*, **46**, 1935
- Watson, J. K. G. 1977a, in *Vibrational Spectra and Structure*, ed. J. Durig, Vol. 6 (Amsterdam: Elsevier), 1
- Watson, J. K. G. 1977b, *J. Mol. Spectrosc.*, **65**, 123
- Woon, D. E. 2002, *ApJ*, **571**, L177
- Woon, D. E., & Dunning, T. H. 1995, *J. Chem. Phys.*, **103**, 4572
- Zaleski, D. P., Seifert, N. A., Steber, A. L., et al. 2013, *ApJ*, **765**, L10
- Zeng, S., Jiménez-Serra, I., Rivilla, V. M., et al. 2018, *MNRAS*, **478**, 2962

## Appendix A: Details of the theoretical calculations

For calculating the equilibrium structures, extrapolation to the complete basis set (CBS) limit was performed for both the Hartree-Fock self-consistent field (HF-SCF) and the valence correlation (evaluated at the frozen-core (fc) CCSD(T) level of theory) terms, using the formulas of Halkier et al. (1999) for the former and the two-parameter correction of Helgaker et al. (1997a) for the latter. At the HF-SCF level of theory, the correlation consistent polarised basis sets cc-pVnZ ( $n = T, Q, 5$ ) of Dunning (1989) and Woon & Dunning (1995) were used, while the fc-CCSD(T) calculations were carried out by using the cc-pVTZ and cc-pVQZ basis sets. For computing the contribution related to the core-valence (CV) electron correlation, the difference between the all-electron (ae) and frozen-core results using the cc-pCVTZ basis set (Woon & Dunning 1995) was used, while the contribution due to the diffuse functions was calculated by employing the aug-cc-pVTZ basis set (Kendall et al. 1992). All these terms were evaluated at the CCSD(T) level of theory. The energies of these two structures were computed using the same approach, but with the cc-pVnZ ( $n = Q, 5, 6$ ) basis sets. The vibrational corrections to both the equilibrium rotational constants were calculated at the fc-MP2 level of theory (Møller & Plesset 1934) using the aug-cc-pVTZ basis set; the same level of theory also provided the anharmonic corrections used to compute the fundamental frequencies reported in Table A.2. The cubic force-field data needed for determining the sextic centrifugal distortion constants were obtained at the CCSD(T) level on the basis of its good accuracy reported in the literature (Pietropolli Charmet et al. 2017b). Nuclear quadrupole coupling constants for the nitrogen atoms were computed at the ae-CCSD(T) level of theory in conjunction with the pw-CV5Z basis set (Dunning 1989; Peterson & Dunning 2002) following the same procedure as previously described (Cazzoli et al. 2011; Pietropolli Charmet et al. 2016).

All the calculations carried out at the CCSD(T) and MP2 levels of theory were performed using the CFOUR<sup>10</sup> suite of

programs and its implementation of analytic second derivatives (Gauß & Stanton 1997), while the sextic centrifugal distortion constants were computed using an appropriate suite of programs (Pietropolli Charmet & Cornaton 2018) and the formulas reported in the literature (Aliev & Watson 1976, 1985; Watson 1977b). A summary of the results provided by the present ab initio calculations is presented in Table A.1 together with the comparison with the values reported in the literature (Sugie et al. 1985; Osman et al. 2014).

Concerning the equilibrium molecular parameters obtained by our calculations, on the basis of previous studies (see, for example Bak et al. 2001), we may estimate an overall accuracy of  $2\text{--}3 \times 10^{-3} \text{ \AA}$  for bond distances. For comparison, the bond lengths reported by Sugie et al. (1985) listed in Table A.1 are generally shorter, while the ones computed by Osman et al. (2014) (listed in the same table) are generally longer. These discrepancies are due to the low level of theory used in these earlier studies. As a matter of fact, the accuracy of molecular equilibrium structures is strongly dependent on the wave function method employed; for example, it is reported that computations carried out at HF level of theory generally underestimate the bond lengths, while CCSD calculations, depending on the basis set used, may predict values that are either too short or too long (Helgaker et al. 1997b).

As an independent test of the overall reliability of the theoretical calculations, one can apply the ab initio zero-point vibrational contributions to the experimentally derived ground state rotational constants and obtain the so-called semi-experimental equilibrium rotational constants. From these quantities, the inertial defect can be estimated yielding  $-6.7 \times 10^{-4} \text{ u \AA}^2$  for Z-PGIM and  $-2.7 \times 10^{-3} \text{ u \AA}^2$  for E-PGIM. These values are very close to zero, as expected for a molecule with planar equilibrium configuration, thus indicating that both the electronic structures and the vibrational dynamics were correctly modelled (McCarthy et al. 2016).

<sup>10</sup> CFOUR, Coupled-Cluster techniques for Computational Chemistry, a quantum-chemical program package written by J.F. Stanton, J. Gauss, L. Cheng, M.E. Harding, D.A. Matthews, P.G. Szalay et al., and the integral packages MOLECULE (J. Almlöf and P.R. Taylor), PROPS (P.R. Taylor), ABACUS (T. Helgaker, H.J. Aa. Jensen, P. Jørgensen, and J. Olsen), and ECP routines by A. V. Mitin and C. van Wüllen. For the current version, see <http://www.cfour.de>

**Table A.1.** Theoretically computed equilibrium geometries<sup>(a)</sup>, dipole moments<sup>(b)</sup>, relative energy<sup>(c)</sup>, and equilibrium rotational constants<sup>(c)</sup> of PGIM isomers and comparison with previous works.

		Z-PGIM			E-PGIM		
		This work	Ref. (1) <sup>(d)</sup>	Ref. (2) <sup>(e)</sup>	This work	Ref. (1) <sup>(d)</sup>	Ref. (2) <sup>(e)</sup>
C≡C	/Å	1.2074	1.1845	1.226	1.2066	1.1838	1.225
C–C	/Å	1.4374	1.4480	1.460	1.4345	1.4444	1.457
C=N	/Å	1.2767	1.2504	1.288	1.2770	1.2506	1.289
H–C	/Å	1.0635	1.0558	1.076	1.0634	1.0557	1.076
C–H	/Å	1.0863	1.0780	1.100	1.0903	1.0827	1.102
N–H	/Å	1.0199	1.0060	1.029	1.0184	1.0046	1.028
∠(C–C–H)	/deg	116.52	115.82		115.54	114.60	
∠(H–C=N)	/deg	118.11	118.38		123.32	123.98	
∠(H–N=C)	/deg	110.49	111.97	109.75	109.92	110.94	109.06
∠(C–C=N)	/deg	125.37	125.80	126.68	121.14	121.42	121.00
$\mu_a$	/D	2.1449	2.39		0.2567	0.23	
$\mu_b$	/D	0.1674	0.26		1.9346	2.13	
$E_0$	/kcal mol <sup>-1</sup>	0.0	0.0	0.0	0.8510	1.037	0.697
$A_e$	/MHz	54525.6766	56884.0		63330.757	65775.0	
$B_e$	/MHz	4876.6255	4924.0		4772.651	4833.0	
$C_e$	/MHz	4476.2794	4531.0		4438.187	4502.0	

**Notes.** <sup>(a)</sup>Extrapolated “best value”, CCSD(T)/CBS+CV. <sup>(b)</sup>Extrapolated CCSD(T)/CBS+CV (absolute values). <sup>(c)</sup>See Appendix A for explanation. <sup>(d)</sup>Ref. (1) is [Sugie et al. \(1985\)](#), computed at the HF/4-31G\* level of theory. <sup>(e)</sup>Ref. (2) is [Osman et al. \(2014\)](#), computed at the CCSD/aug-cc-pVDZ level of theory.

**Table A.2.** Anharmonic frequencies (cm<sup>-1</sup>) for the singly excited vibrational levels of PGIM isomers.

Level	Symmetry	Z-PGIM	E-PGIM
$\nu_1$	A'	3322	3337
$\nu_2$	A'	3275	3286
$\nu_3$	A'	3028	2911
$\nu_4$	A'	2113	2121
$\nu_5$	A'	1592	1605
$\nu_6$	A'	1395	1385
$\nu_7$	A'	1224	1224
$\nu_8$	A'	922	916
$\nu_9$	A'	640	643
$\nu_{10}$	A'	591	596
$\nu_{11}$	A'	211	219
$\nu_{12}$	A''	1099	1074
$\nu_{13}$	A''	817	795
$\nu_{14}$	A''	646	651
$\nu_{15}$	A''	289	285

**Notes.** Harmonic force-field data corrected by cubic and quartic semi-diagonal force constants obtained by fc-MP2 calculations (see text for details).